Image Segmentation of Fluorescence Retinal Images for Photothermal Retinal Prosthetics

By

Anoop Reddi

BA, University of Pittsburgh, 2018

Thesis

Submitted in partial fulfillment of the requirements for the Degree of Master of Science in the Graduate Program of Biotechnology at Brown University

PROVIDENCE, RHODE ISLAND

February 2023

AUTHORIZATION TO LEND AND REPRODUCE THE THESIS

As the sole author of this thesis, I authorize Brown University to lend it to other institutions for the purpose of scholarly research.

Date 1/11/23

Anoop Reddi, Author

I further authorize Brown University to reproduce this thesis by photocopying or other means, in total or in part, at the request of other institutions or individuals for the purpose of scholarly research.

Date 1/11/23

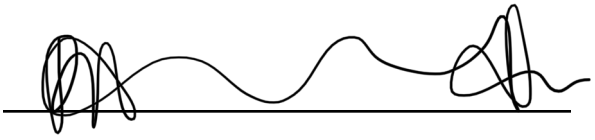

Anoop Reddi, Author

This thesis by Anoop Reddi is accepted in its present form by the Graduate Program in Biotechnology as satisfying the thesis requirements for the degree of Master of Science

Date_____ Signature: _____

Dr. Jonghwan Lee, Advisor

Date_____ Signature: David Borton Digitally signed by David Borton Date: 2022.12.29 18:08:56 -05'00'

Dr. David Borton, Reader

Date 1/6/23 Signature: _____

Dr. Jeffrey Morgan, Reader

Date 1/9/2023 Signature: Edith Mathiowitz

Dr. Edith Mathiowitz, Reader

Approved by the Graduate Council

Date_____ Signature: _____

Dr. Thomas Lewis, Dean of the Graduate School

Acknowledgements

First and foremost, I would like to thank Dr. Jonghwan Lee and the entirety of Lee Lab for providing me with the opportunity to work on this project. With Dr. Lee's guidance, I've learned many invaluable lessons that I will carry with me. He gave me the freedom to explore areas that I like, while pushing me to become a better engineer. I would also like to thank Jiarui Nie for her guidance in the retinal dissection and experimentation parts of this project. Lastly, I would like to thank Brown for accepting me into its community and providing me with the environment and resources that will help me for the rest of my career.

Table of Contents

Abstract

Currently, electrode-based retinal implants are severely limited in the restoration of vision loss. These implants are highly-invasive, limited in resolution, and degrade in utility overtime. A novel, minimally-invasive retinal prosthesis is being developed to overcome such limitations and stimulate retinal neurons to restore vision in blindness. This system uses gold nanorods (AuNRs) and near-infrared (NIR) light to activate retinal neurons by causing temperature changes in the neuronal membranes. A custom experimental setup involving a scanning laser system and a fluorescence imaging system will be used to validate the photothermal activation of retinal neurons ex-vivo before moving on to in-vivo investigations. An important aim in the ex-vivo validation is to determine the number of RGCs activated per unit time by analyzing the images taken by the camera. Our imaging system captures ~1000 retinal neurons, and it is very challenging if not impossible, to manually identify individual cells and obtain their time traces, especially when we have tens of retinal samples and data to analyze. This thesis focuses on implementing various image segmentation algorithms that automatically identify individual cells from a grayscale fluorescence image of a retinal explant and comparing their performance.

Introduction

Retinitis Pigmentosa (RP) is an eye disorder that occurs from the degeneration of the outer layer of the retina, which is a membrane that is highly sensitive to light entering the eye. It's a disorder that affects about 1 in every 3,000-4,000 people, translating to about 110,000 people in the United States and about 2.6 million people around the world that are affected by RP[1].

Despite many efforts in place, no one has developed a cure for the outer retinal degeneration of the retina. Because only the outer retinal layer degenerates, there is potential for restoration of vision using the inner layers of the retina[2]. There are various efforts currently in place to restore vision in RP from optogenetics[3] to stem-cell therapies[4]. Inorganic technologies such as microelectrode-based and photovoltaics are making some progress[5]. Newer, organic technologies are also being developed such as using conjugated polymers and organic photoswitches[6]. However, clinically, the current gold standard remains to be the electrode-based retinal prosthesis.

The electrode-based retinal prosthetic device usually involves a microelectrode array, signal processing, and a head-mounted device to collect incoming light[7]. Specifically, the microelectrode array can be placed in the epiretina, subretina, or the suprachoroidal space. Through electrical stimulation of the retina, the neuronal membrane depolarizes and opens up various ion channels, leading to action potentials. These action potentials can then travel through the optic nerve to the visual cortex for further vision processing, allowing for perception in humans. While the electrode-based retinal prosthetic seems like a sound solution, there are various limitations.

There are glaring disadvantages that make the electrode-based retinal prosthesis limited in its application. One disadvantage is that it is highly-invasive, requiring a surgical implantation of the microelectrode. After the implantation, studies have shown that only after 6 months of implantation, residue resembling macrophage-like tissue developed around 25% of electrodes, which degrades the ability to discharge electrical impulses into the retina[8]. Additionally, electrical impulses can cause damage to the retinal tissue[9]. It is believed that a charge density of less than 100-200 μC/cm^2 is considered safe. But the size of the electrodes that are capable of discharging within that safety limit are relatively large, which limits the visual resolution[9]. The electrode-based retinal prosthetic also has a factor imposing a fundamental limit in the visual resolution: electricity can easily spread within the conductive media in the retina. At present, the electrode-based retinal prosthetic is known to have a resolution of about 150 μm, while a retinal ganglion cell is known to have a diameter of about 10 μm[10]. Because of the spreading of electricity, one electrical impulse can stimulate many neighboring neurons. Other limitations of the electrode-based stimulation include the fixed number of stimulation sites and fixed position of the electrode itself. Once implanted, it becomes impossible without surgical intervention to change the position of the electrode and the area of the retina the electrode stimulates.

The only FDA approved retinal prosthetic device is the Argus II from Second Sight Medical Products[11]. The Argus II is shown to restore a visual field of 22 degrees[12]. The restored visual acuity of the Argus II is 20/1260, which is still worse than the visual acuity of legal blindness, 20/200[13].

Because of these inherent limitations of the electrode-based retinal prosthetics, researchers have started to look for more minimally-invasive, accurate ways to stimulate retinal neurons. One of the avenues involves using infrared (IR) light. About a decade ago, researchers

found IR light to stimulate action potentials in various parts of the nervous system including peripheral[14] and cranial neurons[15], vestibular hair cells[16], cochlear neurons[17], and the heart[18]. IR stimulation is posed to be a better alternative to electrical stimulation. It can be remotely activated, without any implantation required.

IR stimulation causes temperature changes in the neuronal membrane, opening temperature-sensitive ion channels (transient receptor potential cation channel subclass V 1; TRPV1) or generating capacitive currents[19]. For this type of change to occur in the biological membranes, the wavelength must be between 1400-2200 nm[20]. However there are two main limitations to using this wavelength: high heat absorption coefficient and limited penetration depth[20]. Having a high heat absorption coefficient leads to bulk heating. With limited penetration depth, it is difficult for the wavelength to penetrate into the tissue.

To overcome such limitations, near-infrared (NIR) light, with a wavelength between 700-900 nm, will be applied instead. Within this range, the heat absorption coefficient is low enough to avoid bulk heating, and is less likely to damage biological membranes. One caveat to this low heat absorption coefficient is the difficulty to induce enough heat to increase the temperature and cause conformational changes in the neuronal membranes that will eventually trigger action potentials. To get over this barrier, the NIR light will be coupled with gold-nanorods (AuNRs). These AuNRs will absorb NIR light and through localized surface plasmon resonance, generating heat and temperature changes required[21].

NIR light has already shown to have the potential to achieve single-cell resolution, but only in rat hippocampal cultures ex-vivo[22]. To push the boundaries even further and validate single-cell resolution in the retina, a crucial step is to demonstrate a patterned stimulation with NIR laser pulses.

By combining a scanning laser system and a fluorescence microscope, we illuminated NIR laser pulses and imaged retinal ganglion cell (RGC) activity via intracellular Ca^{2+} concentration changes, on retinal explants of genetically-induced blind and genetically-encoded Ca^{2+} indicator GCaMP3 mice. This experiment produced a large number of images as fluorescence video data. Seven days before retinal dissection for this ex-vivo experiment, mice were intravitreally injected AuNRs.

One of the current challenges in the data analysis of these images is to quantify how many RGCs are activated. Our imaging system captures ~1000 retinal neurons, and it is very challenging if not impossible, to manually identify individual cells and obtain their time traces, especially when we have tens of retinal samples and several stimulation parameters per sample. This thesis specifically aims to implement software that automatically identifies individual cells from a grayscale GCaMP image of a retinal explant. To achieve this objective, I prepared retinal tissue from mice, obtained GCaMP images, implemented and applied various image segmentation algorithms to the GCaMP images, and compared their performance.

Methods

Eye Retrieval

The process of eye retrieval begins once death has been confirmed and additional measures, such as cervical dislocation, have been completed. The mouse is then placed in an open zip lock bag and carried to the microscope, where the dissection happens. After taking the mouse out of the bag, gentle pressure is applied to stabilize the head and the eyelids are retracted so that the eyes begin protruding out. In efforts to not damage the eye, the flat edges of the forceps are applied to the superior and inferior parts of the eye. Small amounts of pressure are continuously applied via the forceps so that the eye protrudes further out. Then, without damaging the eye, the forceps are rotated so that the tips enter the orbital space. Once confident, the forceps are used to grasp the eye and gently remove it. A successful removal should produce an eye along with significant residual tissue. The removed eye is then placed in the perfused petri dish.

Retinal Dissection

First, there should not be significant tissue attached to the posterior of the eye. If so, it may need to be removed to minimize the risk of entanglement with the retina. However, retention of surrounding musculature aids significantly in stabilizing the eye when dissecting. The eye should be gently punctured at the intersection of the cornea and sclera (corneal limbus) with the needle, angled such that the tip penetrates towards the cornea. One blade of the micro-dissectors should be inserted through the puncture, proceeding to hemisect the retina. The tips of the blades should be directed slightly towards the sclera to reduce the risk of retinal injury.

Once the hemisection is complete, pressure should be applied with the smooth edge from one of the closed forceps, while grasping and extracting the lens. During this part of the

procedure, if the retina begins to detach from the cornea, the micro-dissectors could be used to free any residual adhesions. If the retina remains attached to the lens, the sclera should be cut into a petal pattern by making four perpendicular cuts. This will free the retina and will allow the retina to flatten. Placing the retina on filter paper can aid in performing these cuts. The surround area has to be free from debris before detaching the retina completely.

After the lens is removed, one tip of each forcep is inserted between the retina and the RPE/sclera. The other tip should be external to the sclera, such that the sclera can be grasped gently and pulled apart, without touching the retina. This tearing motion may need to be repeated several times to completely free the retina. If, for some reason, the retina remains attached, it can typically be gently brushed away using a small paint brush. Then, the retina is cut with four perpendicular cuts such that the retina falls into a flat flower shaped petal.

The retina is transferred gently onto a small piece of filter paper using a paint brush. It should be centered on the paper, carefully ensuring the posterior surface of the retina is adhering to the filter paper. Using the forceps to grasp the filter paper, the retina is gradually elevated out of the perfusion medium. The microscope is refocused as the retina reaches the surface, ensuring that it is as flat as possible. If, for some reason, the retina does appear to be folded, the paint brush can be used to gently brush the fold so that it becomes flat again. The retina and filter paper should remain saturated with solution until the perfusion of the imaging well can be initiated. The filter paper with the retina is then placed in the center of an imaging well. 2mm blots of silicone adhesive is applied to the slide surrounding the filter paper. To secure the filter paper with the retina, a piece of mesh large enough to cover the filter paper is cut and embedded gently on top. Ideally, there should be some tension created across the mesh while securing to

minimize retinal movement, while being careful not to damage the retina. Then the imaging well should be filled with the perfusion solution.

Fluorescence Microscopy

I used the lab-built fluorescence microscope. This microscope consists of a galvano mirror scanner system that projects laser beams onto the retinal explant to stimulate retinal neurons with a desired pattern. The first pattern we tested has a square shape with a size of 100 μm x 100 μm and was projected a total of 10 times each second (i.e. 10 frames/second).

Results

Retinal Dissection and Imaging

Figure 1 presents an example of a dissected retina.

Figure 1. Dissected retina in imaging well. After the retina is dissected and cut into a petal shape, it is placed inside an imaging well for fluorescence imaging.

Figure 2 presents the baseline fluorescence image before image processing. The bright circles represent RGCs via the genetically induced green fluorescence proteins, i.e., GCaMP. The goal of this thesis is to evaluate various image processing approaches to automatically segmenting those bright cells. It should be noted that the image is a baseline image of cells without any neural stimulation.

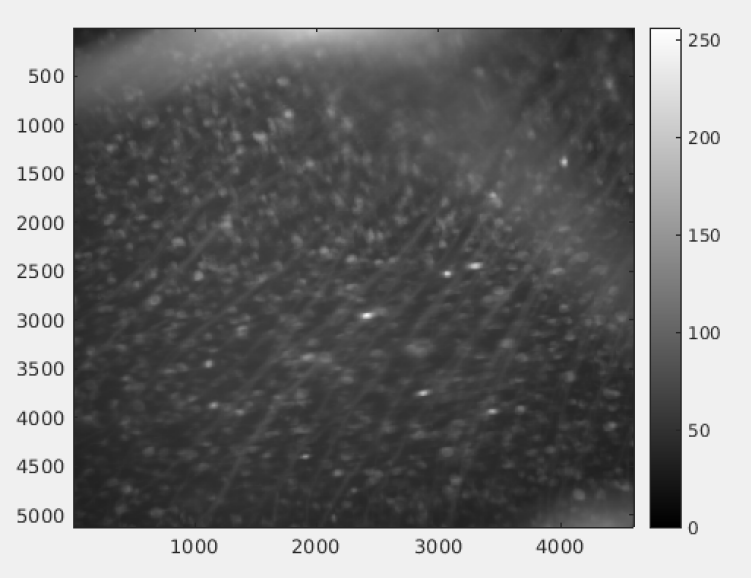

Figure 2. Grayscale image of the retina. The light gray streaks seen in the upper area are the mesh used to hold the retina in place.

To be used as a ground truth in evaluating automatic cell segmentation algorithms, I manually identified retinal cells in the fluorescence image (Figure 3). A total of 384 cells have been identified.

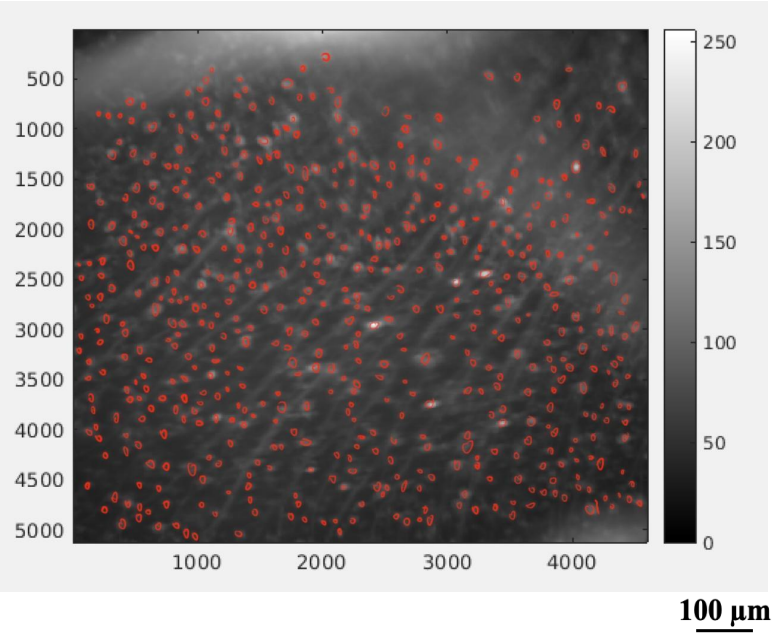

Figure 3. Manual identification of retinal cells. The red circles represent all the retinal cells identified manually in the grayscale image.

Image Segmentation

The aim of my image segmentation is to differentiate retinal cells from the background noise. In general, there are various image segmentation techniques to segment different parts of the images. In this thesis, I tested a range of techniques, including Otsu's method, watershed segmentation, and adaptive thresholding.

Otsu's Method

Otsu's method is an algorithm that separates a grayscale image into two separate classes, foreground and background, by using a single intensity threshold to output a binary image. During traditional image segmentation, this intensity threshold had to be manually determined, requiring a lot of trial and error without much precision and accuracy. Otsu's method is a technique to automatically determine this intensity threshold[23].

The algorithm first processes the input grayscale image and outputs a histogram of the brightness or intensity of all pixels in the image, through a process called histogram equalization. It tries to increase the contrast of the pixels by adjusting the intensity of each pixel. Iterating through each pixel and thresholding value, it calculates the spread of pixel values that fall into either the foreground or background classes. The goal is to determine the smallest variance value between the foreground and background spreads, which can be seen as two different peaks on the histogram[23]. Once it computes the final threshold value of the image, the pixel values greater than the threshold become white, denoting the foreground class, and those that lower than the threshold become black, denoting the background class.

I implemented Otsu's method as a part of the global thresholding algorithm in Matlab and applied it to the fluorescence retina image (Figure 2).

Figure 4. Implementation of otsu's method. The output of implementing Otsu's method is a bimodal image that segmented foreground and background objects based on a global thresholding value.

Marker-Controlled Watershed Segmentation

In image processing, the watershed segmentation technique is based on the concept that the intensities of an image can be thought of as a topographic map, and is used to segment different objects within the image. The bright areas can be visualized as "high" altitudes and dark areas can be visualized as "low" altitudes. The watershed method segments a grayscale image into a topographic representation based on three different factors: minima points, catchment basins, and watershed lines. The main disadvantage of the watershed segmentation is that it is prone to over-segmentation because of the possibility of there being many local minima[24].

A way to get over the over-segmentation problem is by "marking" the foreground objects, which are connected regions of pixels within the foreground objects, and background objects, which are regions of pixels not part of any object. This can be done by the marker-controlled watershed technique[25]. Before performing the watershed transform on the image, the dark regions are segmented by using a segmentation function. The pixels within the regions of each of the objects in the image are identified as the foreground markers. Any pixels outside of the regions of the objects in the image are identified as background markers. Finally, one runs the watershed transform on the image with the modified changes, processing only the regional minima found at the foreground and background marker locations.

I implemented this marker-controlled watershed method in Matlab and applied it to the fluorescence retina image (Fig. 5 and Fig. 6).

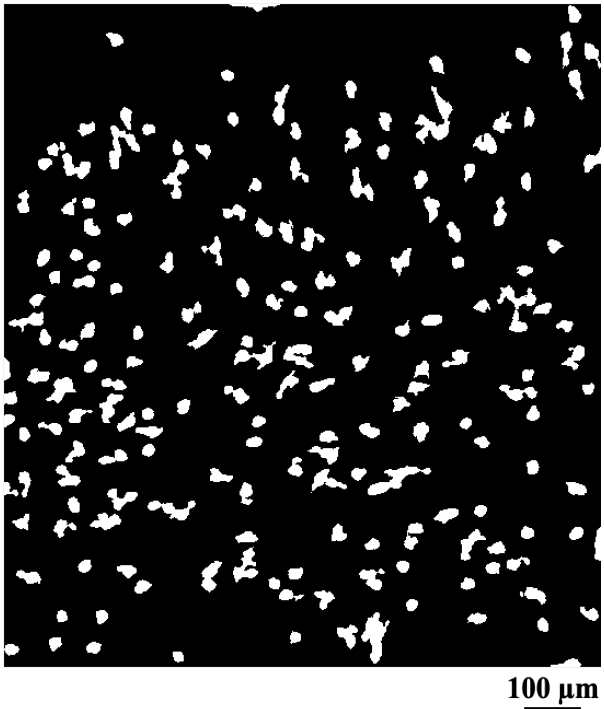

Figure 5. The result of the marker-controlled watershed segmentation.

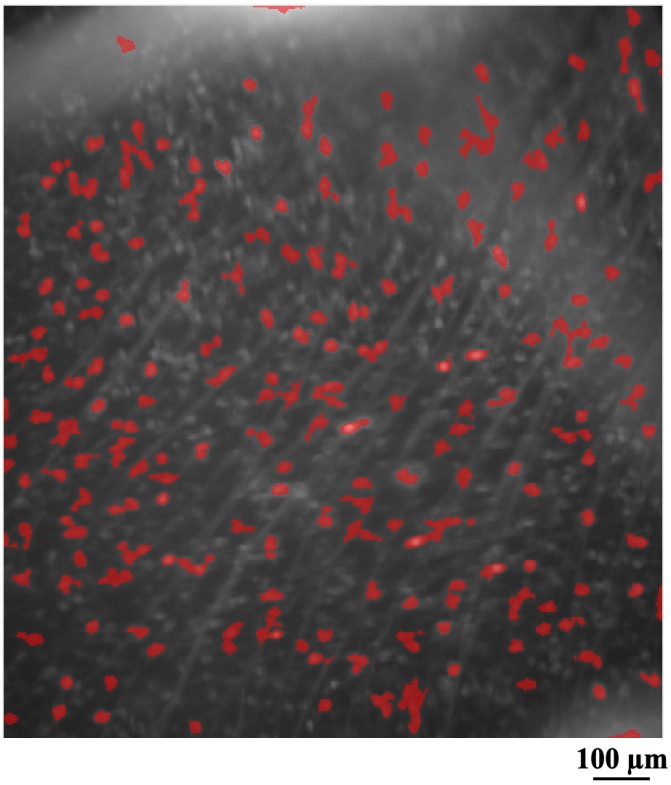

Figure 6. The result of the watershed segmentation superimposed on the original grayscale image.

Adaptive Thresholding

Adaptive thresholding uses local first-order statistics to segment a grayscale image[26]. First-order statistics, from probability theory, refers to the mean. From an image segmentation perspective, adaptive thresholding computes the local mean intensity value of a of a specified neighborhood size[26]. In a related function of Matlab, the sensitivity of this adaptive thresholding can be controlled by an input to the function. The sensitivity value can be set to an arbitrary scalar value between the range of 0 and 1, where the higher the value, the more pixels it denotes to the foreground, and the lower the value, the more pixels it denotes to the background.

I implemented this method, with a sensitivity of 0.5, and a neighborhood size of 300 that specifies the size of the neighborhood around each pixel used for the local first-order statistics.

These optimal values were chosen after going through several trials and errors. The following image was the best result obtained from the various code parameters.

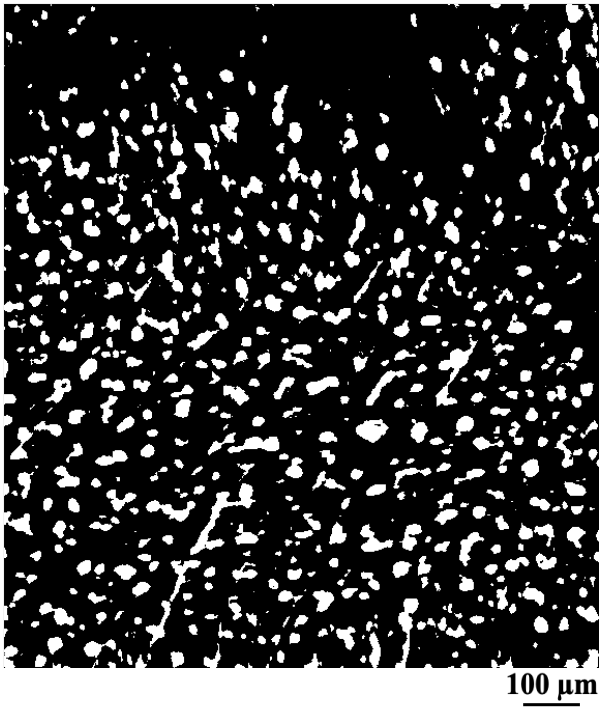

Figure 8. Adaptive threshold applied to grayscale image.

The above method can identify cells, but it is hard to distinguish what is a cell and what is just background noise. Some of the white circular shapes are merged together with other white circular shapes making it hard to identify individual cells separately. To solve this problem, I implemented and applied contrast adjustment methods prior to the adaptive thresholding. Since multiple algorithms exist for image contrast adjustment, I implemented and tested four methods: intensity enhancement, histogram equalization, contrast-limited adaptive histogram equalization (CLAHE), and local laplacian filtering. Figure 9 shows the results of the various image contrast adjustments.

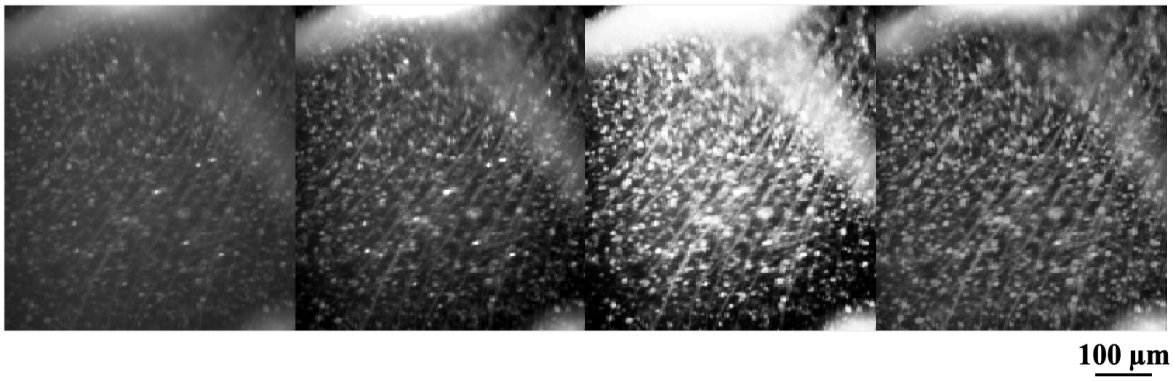

Figure 9. Contrast adjustment methods applied on the grayscale image (1-4). (1) Intensity enhancement . (2) Histogram equalization. (3) Contrast-limited adaptive histogram equalization. (4) Local Laplacian Filtering.

Then, the adaptive threshold method was applied to each result of contrast adjustment.

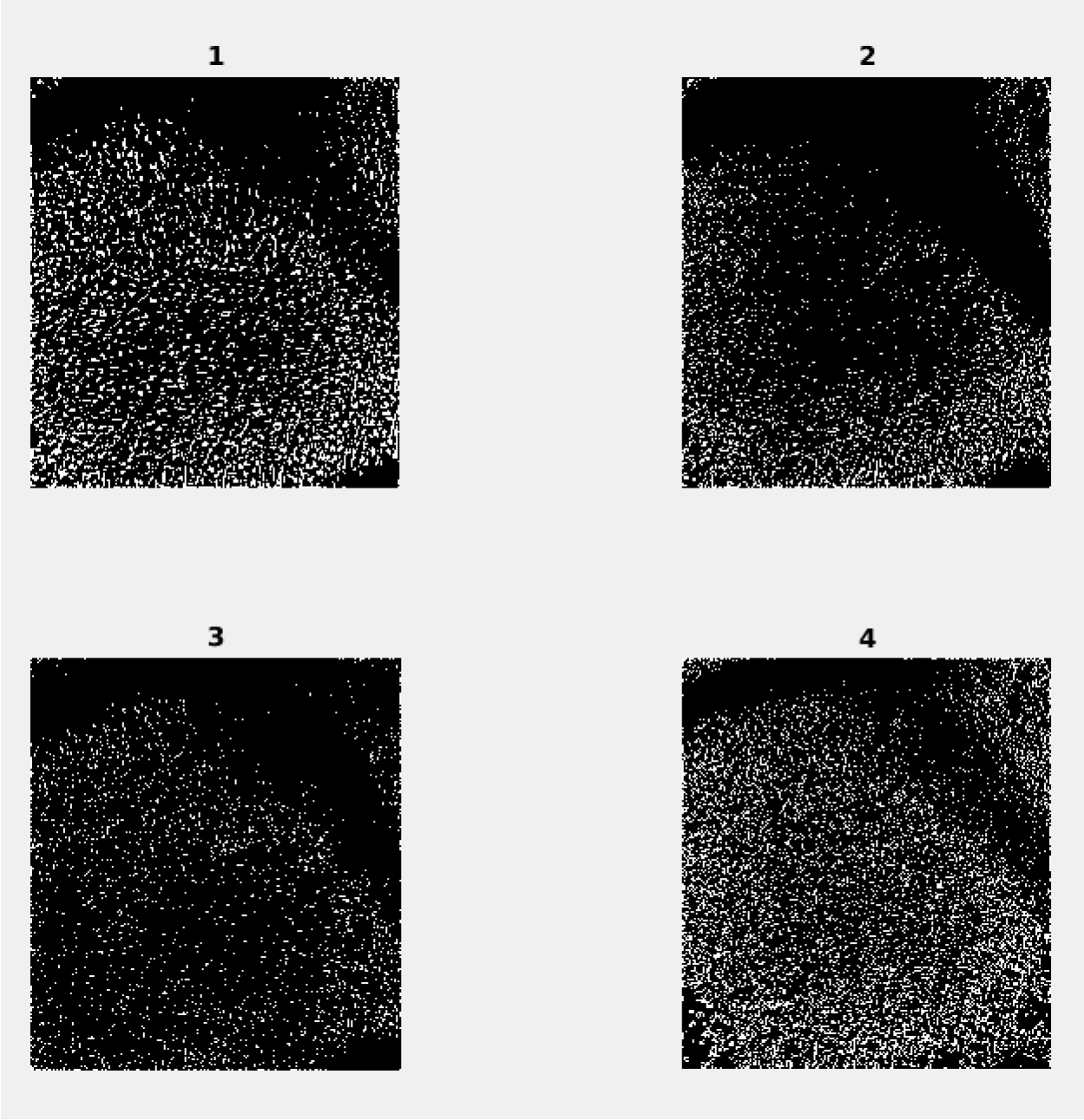

Figure 10. Results of contrast adjustment (1-4). (1) Adaptive threshold on intensity enhancement. (2) Adaptive threshold on histogram equalization. (3) Adaptive threshold on contrast-limited adaptive histogram equalization. (4) Adaptive threshold on local laplacian filtering.

Discussion

All the image segmentation results bore different results to varying degrees of success. Out of all the results, the marker-controlled watershed method fared out to be the better segmentation technique to use, although with certain limitations.

First, Otsu's method had produced the result that was the least effective of all the image segmentation techniques. If compared to the 384 cells that have been manually identified in the grayscale image, there are 347 white, circular objects that may be RGCs. This number is very close to the number of manually identified cells, but when looking at Figure 4, it can clearly be seen that many of the foreground objects are not cells. The reason for this may be that this method takes one thresholding value to segment the image objects into foreground and background. When looking at the original grayscale image, there are many RGCs that can be identified by the naked eye with varying intensities (brightness). Selecting one thresholding value for all pixels may not help the algorithm effectively identify most, if not all, RGCs with varying intensities. In Figure 4, the first object that stands out is the large white streak. When compared with the grayscale image, this can be seen as where the mesh resided, but the algorithm mistook the mesh object and included it when processing the global thresholding value. In return, it ended up placing the mesh object in the foreground objects class. While there are some circular, white objects that may represent RGCs, there are also very large circular, white objects that are too big to definitely conclude as RGCs. This larger circular, white object can be a group of RGCs that the algorithm identified as one white object. All in all, the 347 foreground objects that were counted through this algorithm is not an accurate representation of identified RGCs.

Next, the marker-controlled water segmentation had better results than Otsu's method, but also came with some errors. Firstly, it failed to identify all of the RGCs in the grayscale image visible to the eye. When looking at the comparison (Fig. 5), the algorithm was able to identify 183 foreground objects as cells. For the most part, the algorithm stayed true to the shape of retinal cells as well, although there appears to be about 10-15 minor, irregular white regions as shown in Figure 5. The watershed algorithm also has less of a bleeding effect compared to Otsu's method. The algorithm did a good job at removing the noise in the image, but may have removed certain RGCs as well in the process, thinking those RGCs were noise. Looking at the superimposed image (Fig. 6), there can be some comparison drawn between the bright areas representing RGCs in the original grayscale image and the red regions identified by the algorithm that are supposed to represent identified RGCs. It can be visually seen that certain RGCs on the grayscale image have not been identified. The size of the red regions also appear to be slightly larger than the size of the RGCs on the grayscale image. So, even though the watershed algorithm produced a smaller number of foreground objects than Otsu's method, the morphology and size of most of them are very similar to those of RGCs when visually inspected. Thus, this method appropriately identified cells, but only with 50% accuracy.

When applying the adaptive threshold method, I obtained five different results, one without contrast adjustment filters and four with various contrast adjustment filters. Out of the five results, the adaptive threshold used without any contrast adjustment filter (Fig. 8) obtained the best result. Starting with the results with contrast adjustment filters, when comparing Figures 10.1-10.4 with the original grayscale image, it can be seen visually that there are many white objects detected, much smaller than the RGCs on the grayscale image. In fact, the results get progressively worse when going from Figure 10.1 to Figure 10.4. This was an unexpected result:

Enhancing the image contrast produces worse segmentation. It seems because, when looking at contrast adjustments in Figures 9.1-9.3, each subsequent contrast adjustment intensifies the grayscale image more than the previous. So, on the grayscale image, as the intensity of the white regions increases, the adaptive threshold is more prone to picking up more and more noise. Figure 9.4 used local laplacian filtering and did not have as much contrast adjustment. Interestingly, when looking at Figure 10.4, having applied adaptive thresholding on top of local laplacian filtering, produced the worst result out of the four, picking the most noise. Visually, for all of the results, it was difficult to distinguish whether the white objects are RGCs or noise. Only Figure 8 seems to have the least noise and the best size correlation between the foreground objects and true RGCs.

Comparing Figure 8 to the other image segmentation methods used, it seems to have produced better results compared to Otsu's method, but worse results compared to the marker-controlled watershed method. Unlike Otsu's method, adaptive thresholding seemed to successfully segment the mesh into the background. Adaptive thresholding was also more stable with the segmentation of the size and shape of the white objects. The white objects segmented with Otsu's method had a "streak-like" feature to them. However, when compared to the watershed segmentation, adaptive threshold had more white objets segmented, as it picked up more noise. Quantitatively, the adaptive threshold identified around 951 foreground, white objects, which is a much higher number compared to the total 384 RGCs identified manually (Fig. 3). However, it is highly unlikely that all of the 951 objects are RGCs. It is hard to discriminate between white objects as RGCs versus noise. Watershed segmentation was much more controlled in its white object segmentation, with respect to its lack of noise it picked up and the size and shape of the white objects.

The main drawback of the adaptive thresholding algorithm is it is difficult to assess whether the white regions are RGCs or noise. This algorithm also identified white regions that bleed into other white regions, just like Otsu's method, making it difficult to segment individual RGCs separately. The added image enhancement seemed to add to the noise that the algorithm picked up. Interestingly, even with identification of the noise, the algorithm did manage to disregard the light gray streaks shown in the grayscale image similar to the watershed method.

The reason why adaptive thresholding produced worse results than the watershed segmentation is likely because it calculates a thresholding value for smaller regions of the image as opposed to the entire image. This allows the algorithm to focus on the thresholding value of each of the smaller regions one at a time, making it better than the Otsu's method. However, having a much more localized strategy to segment the image may be less effective than the watershed algorithm because the intensities of the white areas of the original grayscale image have variations. For each localized region, the algorithm may have mistaken noise for RGCs.

Overall, the marker-controlled watershed segmentation worked the best, identifying 183 foreground objects as cells, the most among all the other algorithms. The marker-controlled watershed segmentation seemed to work the best because it is shown to work best with segmenting objects that have closed contours[27]. In the grayscale image, the RGCs have definite boundaries, albeit irregular boundaries, to them, making this method ideal for segmentation.

While the presented result is promising, there are certain ways the algorithm could be refined. From the manual count of 384 RGCs, 183 objects that the algorithm identified is only about 48%. Reminding that the major objective of this software is to find a way to distinguish between RGCs and noise, informing the algorithm of a known size of the RGCs would help. This

way, anything that is smaller than the reasonable size of RGCs can be considered as noise and be disregarded by the algorithm. Much more advanced techniques can be merged with the watershed segmentation, such as wavelet transforms[28], morphological dilation and erosion, to improve results as well[29].

One weakness in this thesis is the using only one fluorescence image to test the various image segmentation methods. If multiple fluorescence images have been tested with the same algorithms, there is a chance that another method might have worked better than the watershed segmentation method. Another weakness in this thesis is that the count used for the ground truth fluorescence image remains subjective because it uses the perspective of one person. If another person analyzed it, the count for the ground truth could have been different.

This thesis also calls into question the number of cells that have to be identified to qualify for the next stage of the project. How many cells identified are good enough? Does the algorithm need to identify every single cell in the fluorescence image to move forward? How does each algorithm compare to another? To measure performance of algorithms with each other, a metric of evaluation called the Area Under the Curve - Receiver Operating Characteristics (AUC-ROC) curve can be used[30].

The benefit of using an AUC-ROC curve is that it objectively measures the performances of the algorithms. One of the main drawbacks of the algorithms tested was the uncertainty in spotting the difference between RGCs and noise. Instead of going by an accuracy metric, the true positive rate (TPR) and false positive rate (FPR) can be calculated. In the case of this thesis, the true positive rate is the number of white objects that were correctly identified as RGCs over the total number of identified objects. The FPR is the number of white objects that were incorrectly

segmented as background noise over the total number of objects segmented as background noise. The ideal conditions we want is a high TPR, because we want to correctly identify as many RGCs as possible, and a low FPR, because we want to limit the number of white objects that are incorrectly segmented as background noise. The ROC curve is obtained by plotting the TPR on the y-axis and the FPR on the x-axis. With this curve we can find a threshold point that allows us to more objectively determine the number of cells that are identified by an algorithm. Since we want to attain the highest TPR and the lowest FPR possible, we can look at the AUC under the ROC curve and figure out for which threshold point results in the largest area[31].

Conclusion

There are three main limitations to the current electrode-based retinal prosthesis: the invasive nature of the microelectrode, restrictions with location and size, and resolution of restored vision. The minimally-invasive, photothermal retinal prosthesis system has a potential to overcome these limitations. An essential component of this system is the activation of multiple retinal neurons according to an induced spatial pattern representing external visual stimuli. To achieve this, a crucial step involves validating ex-vivo that RGCs are activated according to the projected pattern of laser light. This requires a process to automatically segment the retinal neurons in fluorescence images to determine exactly how RGCs are being activated.

Out of all the image segmentation techniques that were experimented with, marker-controlled watershed segmentation worked the best at identifying regions of the image where there may be RGCs. But the result showed margins of improvement. The algorithm needs to be much more precise in identifying more RGCs that reside in the grayscale image, while segmenting out the noise as well. So far it only identified 48% of the total RGCs identified

manually in the grayscale image. On top of that it needs to precisely define the approximate shape of the RGC.

There are many avenues to pursue in the future from this point. Image segmentation is a rapidly changing field with many new methods and algorithms being constantly developed. There are also many existing segmentation techniques that haven't been explored in this thesis. K-means clustering[32] based image segmentation, graph-based segmentation such as lazy snapping[33], binary image segmentation using fast marching method, and many others exist that can refine our results even further[34].

In order for this AuNR enhanced, NIR stimulating retinal prosthesis project to proceed to the next steps for human application, it is imperative to develop image segmentation software to automatically detect and segment RGCs from a large set of ex-vivo validation data. It will give crucial evidence that patterned laser stimulation can activate multiple neurons in the retina.

References

[1] O'Neal TB, Luther EE. Retinitis Pigmentosa. [Updated 2022 Aug 8]. In: StatPearls [Internet]. Treasure Island (FL): StatPearls Publishing; 2022 Jan-. Available from: https://www.ncbi.nlm.nih.gov/books/NBK519518/

[2] Margalit, E. and Sadda, S.R. (2003), Retinal and Optic Nerve Diseases. Artificial Organs, 27: 963-974. https://doi.org/10.1046/j.1525-1594.2003.07304.x

[3] Busskamp V, Roska B. Optogenetic approaches to restoring visual function in retinitis pigmentosa. Curr Opin Neurobiol. 2011 Dec;21(6):942-6. doi: 10.1016/j.conb.2011.06.001. Epub 2011 Jun 25. PMID: 21708457.

[4] Garg A, Yang J, Lee W, Tsang SH. Stem Cell Therapies in Retinal Disorders. Cells. 2017 Feb 2;6(1):4. doi: 10.3390/cells6010004. PMID: 28157165; PMCID: PMC5371869.

[5] Zrenner E. Will retinal implants restore vision? Science. 2002 Feb 8;295(5557):1022-5. doi: 10.1126/science.1067996. Erratum in: Science 2002 Mar 22;295(5563):2213. PMID: 11834821.

[6] Benfenati, F., Lanzani, G. New technologies for developing second generation retinal prostheses. *Lab Anim* 47, 71–75 (2018). https://doi.org/10.1038/s41684-018-0003-1

[7] Weiland JD, Walston ST, Humayun MS. Electrical Stimulation of the Retina to Produce Artificial Vision. Annu Rev Vis Sci. 2016 Oct 14;2:273-294. doi: 10.1146/annurev-vision-111815-114425. PMID: 28532361.

[8] Polikov, Vadim S., et al. “Response of Brain Tissue to Chronically Implanted Neural Electrodes.” *Journal of Neuroscience Methods*, vol. 148, no. 1, 2005, pp. 1–18., https://doi.org/10.1016/j.jneumeth.2005.08.015.

[9] Jessica O. Winter, Stuart F. Cogan & Joseph F. Rizzo (2007) Retinal prostheses: current challenges and future outlook, Journal of Biomaterials Science, Polymer Edition, 18:8, 1031-1055, DOI: 10.1163/156856207781494403

[10] M. R. Behrend, A. K. Ahuja, M. S. Humayun, R. H. Chow and J. D. Weiland, "Resolution of the Epiretinal Prosthesis is not Limited by Electrode Size," in IEEE Transactions on Neural Systems and Rehabilitation Engineering, vol. 19, no. 4, pp. 436-442, Aug. 2011, doi: 10.1109/TNSRE.2011.2140132.

[11] Ayton, Lauren N., et al. “An Update on Retinal Prostheses.” *Clinical Neurophysiology*, vol. 131, no. 6, 2020, pp. 1383–1398., https://doi.org/10.1016/j.clinph.2019.11.029.

[12] H Christiaan Stronks & Gislin Dagnelie (2014) The functional performance of the Argus II retinal prosthesis,Expert Review of Medical Devices, 11:1, 23-30, DOI: 10.1586/17434440.2014.862494

[13] Humayun, M. S., Dorn, J. D., da Cruz, L., Dagnelie, G., Sahel, J.-A., Stanga, P. E., Cideciyan, A. V., Duncan, J. L., Eliott, D., Filley, E., Ho, A. C., Santos, A., Safran, A. B., Arditi, A., Del Priore, L. V., & Greenberg, R. J. (2012). Interim results from the International Trial of Second Sight's visual prosthesis. *Ophthalmology*, *119*(4), 779–788. https://doi.org/10.1016/j.ophtha.2011.09.028

[14] Wells, J., Konrad, P., Kao, C., Jansen, E. D. & Mahadevan-Jansen, A. Pulsed laser versus electrical energy for peripheral nerve stimulation. J. Neurosci. Methods 163, 326–337 (2007).

[15] Teudt, I. U., Nevel, A. E., Izzo, A. D., Walsh Jr, J. T. & Richter, C. Optical stimulation of the facial nerve: a new monitoring technique? Laryngoscope 117, 1641–1647 (2007).

[16] Rajguru, S. M., Richter, C., Matic, A. I., Holstein, G. R., Highstein, S. M., Dittami, G. M. & Rabbitt, R. D. Infrared photostimulation of the crista ampullaris. J. Physiol. 589, 1283–1294 (2011).

[17] Izzo, A. D., Walsh Jr, J. T., Ralph, H., Webb, J., Bendett, M., Wells, J. & Richter, C.-P. Laser stimulation of auditory neurons: effect of shorter pulse duration and penetration depth. Biophys. J. 94, 3159–3166 (2008).

[18] Jenkins, M. W., Duke, A. R., Gu, S., Doughman, Y., Chiel, H. J., Fujioka, H., Watanabe, M., Jansen, E. D. & Rollins, A. M. Optical pacing of the embryonic heart. Nat. Photonics 4, 623 (2010).

[19] Albert, E. S., Bec, J. M., Desmadryl, G., Chekroud, K., Travo, C., Gaboyard, S., Bardin, F., Marc, I., Dumas, M., Lenaers, G., Hamel, C., Muller, A. & Chabbert, C. TRPV4 channels mediate the infrared laser-evoked response in sensory neurons. J. Neurophysiol. 107, 3227–3234 (2012).

[20] Wells, J.D., Thomsen, S., Whitaker, P., Jansen, E.D., Kao, C.C., Konrad, P.E. and Mahadevan-Jansen, A. (2007), Optically mediated nerve stimulation: Identification of injury thresholds. Lasers Surg. Med., 39: 513-526. https://doi.org/10.1002/lsm.20522

[21] Hutter, E., and J. H. Fendler. “Exploitation of Localized Surface Plasmon Resonance.” Advanced Materials, vol. 16, no. 19, 2004, pp. 1685–1706., https://doi.org/10.1002/adma.200400271.

[22] Yong, J., Needham, K., Brown, W. G. A., Nayagam, B. A., McArthur, S. L., Yu, A. & Stoddart, P. R. Gold‐Nanorod‐Assisted Near‐Infrared Stimulation of Primary Auditory Neurons. Adv. Healthc. Mater. 3, 1862–1868 (2014).

[23] Bangare, Sunil L., et al. "Reviewing Otsu’s method for image thresholding." *International Journal of Applied Engineering Research* 10.9 (2015): 21777-21783.

[24] Amanpreet and Ashish Verma. “The Marker-Based Watershed Segmentation- A Review.” (2013).

[25] “Watershed.” *MATLAB & Simulink Example*, https://www.mathworks.com/help/images/marker-controlled-watershed-segmentation.html.

[26] The MathWorks, Inc. (n.d.). *Adaptive image threshold using local first-order statistics - MATLAB*. MathWorks. Retrieved from https://www.mathworks.com/help/images/ref/adaptthresh.html

[27] K. Parvati, B. S. Prakasa Rao, M. Mariya Das, "Image Segmentation Using Gray-Scale Morphology and Marker-Controlled Watershed Transformation", *Discrete Dynamics in Nature and Society*, vol. 2008, Article ID 384346, 8 pages, 2008. https://doi.org/10.1155/2008/384346

[28] Gao, Jianqiang, et al. “A Wavelet Transform-Based Image Segmentation Method.” *Optik*, vol. 208, 2020, p. 164123., https://doi.org/10.1016/j.ijleo.2019.164123.

[29] “Types of Morphological Operations.” *MATLAB & Simulink*, https://www.mathworks.com/help/images/morphological-dilation-and-erosion.html.

[30] Hanley, James A., and Barbara J. McNeil. "The meaning and use of the area under a receiver operating characteristic (ROC) curve." *Radiology* 143.1 (1982): 29-36.

[31] Hoo ZH, Candlish J, Teare D. “What is an ROC curve?” *Emergency Medicine Journal* 2017;34:357-359.

[32] Mittal, H., Pandey, A.C., Saraswat, M. *et al.* A comprehensive survey of image segmentation: clustering methods, performance parameters, and benchmark datasets.*Multimed Tools Appl* 81, 35001–35026 (2022). https://doi.org/10.1007/s11042-021-10594-9

[33] Yin Li, Jian Sun, Chi-Keung Tang, and Heung-Yeung Shum. 2004. Lazy snapping. ACM Trans. Graph. 23, 3 (August 2004), 303–308. https://doi.org/10.1145/1015706.1015719

[34] Chopp, David L. “Some Improvements of the Fast Marching Method.” *SIAM Journal on Scientific Computing*, vol. 23, no. 1, 2001, pp. 230–244., https://doi.org/10.1137/s106482750037617x.